Integrated Human-Virus Metabolic Modelling Predicts Host-Based Antiviral Targets Against Chikungunya, Dengue and Zika Viruses

Sean Aller[1], Andrew E. Scott[2], Mitali Sarkar-Tyson[2,3], and Orkun S. Soyer[1,*]

[1] School of Life Sciences, Gibbet Hill Campus, University of Warwick, Coventry, CV4 7ES, UK. [2] Defence Science and Technology Laboratory (Dstl), Porton Down, Salisbury, SP4 0JQ, UK. [3]Marshall Center for Infectious Disease Research and Training, School of Biomedical Sciences , University of Western Australia, Perth, Australia. [*] Corresponding author

ABSTRACT

Current and reoccurring viral epidemic outbreaks such as those caused by Zika virus illustrate the need for rapid development of antivirals. Such development would be immensely facilitated by computational approaches that can provide experimentally testable predictions for possible antiviral strategies. A key factor that has not been considered fully to date in the study of antiviral targets is the high dependence of viruses to their host metabolism for reproduction. Here, we focus on this dependence and develop a stoichiometric, genome-scale metabolic model that integrates human macrophage cell metabolism with the biochemical demands arising from virus production. Focusing this approach to currently epidemic viruses Chikungunya, Dengue and Zika, we find that each virus causes specific alterations in the host metabolic flux towards fulfilling their individual biochemical demands as predicted by their genome and capsid structure. Subsequent analysis of this integrated model allows us to predict a set of host reactions, which when constrained can inhibit virus production. We show that this prediction recovers most of the known targets of existing antiviral drugs, while highlighting a set of hitherto unexplored reactions with either broad or virus specific antiviral potential. Thus, this computational approach allows rapid generation of experimentally testable hypotheses for novel antiviral targets within a host.

SIGNIFICANCE STATEMENT

A key challenge in combatting any new and emerging virus outbreaks is rapid drug development. In particular, generation of experimentally testable hypotheses through computational approaches is mostly lacking. Here, we address this gap by developing host-virus metabolic models for three viruses that cause current (or previously) epidemic viral outbreaks. We develop viral biomass functions using information from their genomes and physical structure, and incorporate these within a genome-scale metabolic model of human macrophage cells. The resulting integrated model allows us to predict host reactions, which when blocked, stop the system from attaining optimal viral production. These predictions recover currently known antiviral targets within human cells, and highlight a set of new reactions that are hitherto not explored for antiviral capacity.

INTRODUCTION

Rapid development of antiviral drugs for emerging and re-emerging viruses, such as the Zika virus, remains a significant challenge (1, 2). Given that virus production within a host is intertwined with host immune response and metabolism (3), it is suggested that novel development of antivirals should take into account host processes (4, 5). Indeed, viruses are entirely dependent on their hosts' cellular resources for their replication. This is highlighted by observed variations in virus production levels correlating with cell-to-cell variance in growth rate and phase (6), as well as virus infection leading to changes in host metabolism (7). In particular, virus infection leads to significant metabolic alterations in the host, in some cases resulting in up to 3-fold increase in glycolysis rates (7-9) and changes in ATP production rates (6). This observation can be seen as an emergent property of the combined host-virus metabolic system and could be related to changes in host cellular demands arising from viral production (10, 11). More specifically, alterations in host metabolism upon

51 infection can be understood as either viruses actively manipulating the host system to their
52 advantage (12), or the additional draw of metabolic components for viral production simply
53 resulting in a re-arrangement of host metabolic fluxes.
54
55 Regardless of its cause, the entanglement between host metabolism and viral production
56 opens up the possibility to perturb the former, as a way of limiting the latter (9, 12, 13). To
57 explore this possibility and towards understanding the potential interplay between host
58 metabolism and the additional 'virus demand' on it, stoichiometric genome scale metabolic
59 models and their optimisation through flux balance analysis (FBA) can provide ideal starting
60 points as they are demonstrated to allow analysis of cellular physiology as an interconnected
61 system (14, 15). Integration of virus production in a host metabolic model has already been
62 utilised to study the infection of bacteria with phage, indicating the presence of metabolic
63 limitations on phage replication depending on host's metabolic environment (16). While this
64 type of stoichiometric metabolic analysis can potentially be applied to any host-virus pair, it
65 is particularly suited to *Alpha*- and *Flavi*-viruses. The rather simple physical and genomic
66 structure of these viruses (17, 18) allow straightforward construction of a pseudo biochemical
67 reaction representing their production from constituting parts. This pseudo reaction can then
68 subsequently be incorporated into a genome-scale metabolic model of any host.
69
70 Here, we develop and apply such an FBA approach to analyse host-virus metabolic
71 entanglement. Using a stoichiometric metabolic model of a human macrophage cell, we
72 establish an integrated virus-macrophage metabolic model for three viruses causing current
73 (or previously) epidemic outbreaks: Chikungunya virus (CHIKV); Dengue virus (DENV);
74 and Zika virus (ZIKV). These are representatives of the virus genera *Alpha*- (CHIKV) and
75 *Flavi-virus* (DENV, ZIKV), which are positive-sense single-strand RNA-viruses with rather

simple physical structures (17, 18). Viruses of both families have been observed to infect monocyte derived macrophage cell lines (19-21) and are usually transmitted to humans via arthropod vectors, the most common being mosquitos of the *Aedes* genus (22, 23). By analysing the integrated metabolic model, we find that viral production results in significant alterations in host metabolic fluxes. Subsequent analysis of this integrated model through linear optimisation allows us to predict a set of host reactions, which when constrained can inhibit virus production within the macrophage metabolic system. We show that this prediction recovers most of the known targets of existing antiviral drugs, while highlighting a set of hitherto unexplored reactions that either limit virus activity broadly or for a specific virus. Thus, this computational approach allows rapid generation of experimentally testable hypotheses for novel antiviral targets within a host cell.

RESULTS

Host metabolism displays alternative host- and viral-optimal states. We first used the integrated virus-macrophage stoichiometric metabolic model to interrogate potential changes in host metabolism upon virus infection. To do so, we considered two idealised scenarios; one in which the metabolic system is optimised for the functional requirements of the host cell as determined by a maintenance related biomass reaction (24) (host-optimal state), and another in which the metabolic system is optimised solely for a biomass reaction that represents the production of virus particles and that is derived from viral genomes (virus-optimal state) (see *Methods* and Figure S1 for details of virus biomass calculations). These two states provide the theoretical extremes of a continuum of metabolic states that can arise during virus infection. Whilst the first scenario aims to represent the normal physiological state of macrophage cells, the second state represents a thought experiment of the host metabolic fluxes being set for maximizing virus production.

To compare the host- and virus-optimal states of the model, we analyse the metabolic fluxes directly feeding into the biomass pseudo reaction (see *Supplementary Files S1* for biomass reactions and *S2* for flux values and ranges). As expected from linear optimisation, we find that these fluxes reflect the stoichiometric differences in the amino acid and nucleotide requirements of the host cell and the virus, thus achieving perfect fulfilment of host or virus biomass requirements. We conclude that stoichiometric differences in metabolic requirements for virus production vs. host maintenance, as summarised in Figure 1, result in different metabolic flux states of the host model.

The flux variability allowed in the system varies for viral- and host optima, indicating significant physiological changes in the host metabolism to meet viral demands. To understand how the flux changes at biomass level affect the metabolic system, we calculated the allowed flux variability for individual reactions in the model using either host- or virus-based optimisation (see *Methods*). Flux variability analysis (FVA) allows for a more robust analysis of different states of the model, compared to simply calculating optimal flux sets, which are shown to be subject to inaccuracies inherent in linear solvers used in flux balance analysis (25). We find that the median of the allowed optimal metabolic flux ranges, between host- and virus-optimal states, shows significant changes across subprocesses (Figure 2 and *Supplementary File S2*). In particular, the virus-optimal state displays significantly increased median flux for reactions associated with lipid metabolism and nucleotide biosynthesis, and significantly decreased flux for reactions associated with fatty acid biosynthesis and transport (including intracellular transport reactions). Besides these general overall trends across subprocesses, the virus-optimal state displays both increased or decreased median flux for specific reactions within each subprocess (see pie charts in Figure 2). These changes are in accordance with downstream requirements for fulfilling biomass requirements, and relate to

interconnections among sub-processes. For example, the reactions from the lipid metabolism subprocess that show the most increase in their median fluxes (compared to host) involve ADP/ATP and phosphor, which are metabolites that link directly into the reactions of the nucleotide biosynthesis subprocess (and feeding into increased nucleotide requirement in the virus, see Figure 1).

The specific changes in the allowed flux ranges also highlight potential physiological changes. As an illustrative example, we show the extent of changes within the glycolysis pathway, where allowed flux ranges that can sustain virus-optima are wider compared to those that can sustain host-optima (Figure 2). The allowed ranges for glucose and oxygen uptake indicate that virus-optima can be sustained even under low uptake fluxes, indicative of the potential feasibility of anaerobic metabolism still sustaining virus production (26). Taken together, this comparison of host- and virus-optimal states show that the differences within the stoichiometric requirements of the different viruses and between the host cause large-scale alterations in the host metabolic fluxes.

Enforcing host-optimal flux ranges on individual reactions in the model predicts antiviral targets that can suppress viral production. As the host-optimal and virus-optimal flux ranges within the integrated model differ, we hypothesize that the model can be constrained in a way to limit viral production (see *Methods*). To test and utilise this hypothesis, we use the integrated stoichiometric model to identify the host reactions, which, when constrained limit virus production the most. This analysis can be implemented in different ways, for example through constraining of flux values to zero (i.e. reaction 'knock-outs'). Applying such knock-outs, we find several reactions that limit virus-optima, but all of these also results in significant reduction in host-optima (*Supplementary File S3*). To identify if there any reactions that can perturb virus production, whilst maintaining the host viability,

we constrained reaction fluxes to ranges that are derived from the FVA described above. In particular, we identified flux ranges that still allowed for the attainment of the host-optimal state, but were outside of the range allowed by the virus-optimal state (see *Methods*).

This approach highlights a set of reactions that result in different levels of reductions in the virus optima of CHIKV, DENV or ZIKV, while not affecting the host-optima (as expected from the way we set the flux constraints, see *Methods*). We identify 29 reactions that can reduce the virus optima to below 80% of the original value for at least one virus (*Supplementary File S4*). Interestingly, many of these 29 reactions are interconnected, and are involved in the *de novo* synthesis of RNA nucleotides (both purine and pyrimidine pathways) and in amino acid interconversions (Figure 3). Particular examples include reactions directly involved in the synthesis of adenosine, guanosine and uridine/cytidine nucleotides, and upstream reactions such as those involving inosine monophosphate (IMP) and orotidine monophosphate (OMP).

These identified reactions are potential antiviral targets, in the sense that altering their fluxes can limit virus production within the host. Thus, we explored if these reactions match with known antiviral drug targets. Performing a literature analysis, we found that there are currently 10 antivirals, specific to RNA-viruses, and these target only 5 unique metabolic enzymes (see *Supplementary Table 1*). Of these 5 drug targets (and the associated drugs) one has been experimentally verified to be effective against CHIKV (Inositol-5'-monophosphate dehydrogenase; *IMPD*) (27); and another against DENV (Dihydroorotate Dehydrogenase; *DHORD9*) (28). Whilst the other three targets have been verified to be effective against a number of RNA viruses (29), they are yet to be tested against CHIKV, DENV and ZIKV.

We found that out of these 5 known antiviral targets, all are implicated in our analysis. The three known antiviral target reactions involving the genes *IMPD* (27); *DHORD9* (28); and Orotidine-5'-phosphate Decarboxylase (*OMPDC*) (29) are found to

perturb virus optima for all viruses (Figure 3). The antiviral target S-adenosylhomocysteine hydrolase (*AHC*) (29) is predicted to effect only CHIKV optima, and only to a level higher than the 80% cut-off we used in the above analysis (we note that setting *AHC* reaction flux to zero abolishes virus growth for all three viruses (see *Supplementary File S3*)). Finally, CTP synthase, which has been indicated to exhibit an effect on several RNA viruses (29), is included in the model as two reactions which perform the same reaction utilising either ammonia (mediated by *CTPS1*) or glutamine (mediated by *CTPS2*) as a nitrogen source (30) and therefore not highlighted in our initial flux enforcement analysis focusing on single reactions. When we constrain both reactions associated with these two reactions simultaneously at host-derived flux ranges, a reduction in all virus optima is observed.

Identified flux enforcement effects are significant and arise from differences in host- and virus- stoichiometric requirements. The above results provide support for using integrated host-virus metabolic models for identifying host-based antiviral targets. However, any analysis based on stoichiometric metabolic flux optimisation, as done here, can be dependent on details of model implementation and assumptions (25). For example, while the host metabolic model and the biomass function that it incorporates are verified against experimental data (24), the model still assumes a specific media composition and uptake fluxes. To test if our predictions are robust against key assumptions in the model, we analysed the effects of variations in the media composition for the host model and the genomic sequence of the virus on the antiviral target prediction. In particular, we repeated the above analysis for 1000 alternative media uptake fluxes and 1000 point mutations for each of the three virus genomes, affecting the final virus biomass (see *Methods*). We found that the list of reactions with highest impact on virus biomass, while maintaining the host biomass,

200 are qualitatively not altered with these changes in the model structure and we still recover
201 known broad antiviral targets (*Supplementary File S5* and Figures S2-4).
202 To further probe the significance of these reactions as effectors of virus production, we
203 generated 6000 randomised virus biomass compositions using the three original virus
204 biomass functions as a starting point (see *Methods*). Repeating the enforcement analysis for
205 this randomized set thus allowed us to generate a distribution of effects of reactions on virus-
206 like particle production in the host system, thus acting as a null hypothesis. Results from the
207 enforcement of the original unaltered virus sequences, as well as the point mutated virus
208 sequences (mentioned above), were compared against the population of 'randomised' viruses
209 to assess the significance of the antiviral effect (see *Methods*). This allows derivation of a
210 significance value for the effects resulting from each reaction, when the flux enforcement
211 analysis is applied on it. When we rank reactions according to the significance of their
212 effects, we find that the list of reactions shown in *Supplementary File S4* are ranked among
213 the top (*Supplementary Files S5* and *S6*), i.e. these reactions cause biomass reduction for each
214 virus that is statistically significant when compared to their effects on randomised virus-like
215 biomass functions. There are a couple of exceptions only in the case of ZIKV, where the
216 reactions mediated by cystathionine g-lyase (*CYSTGL*) and cystathionine beta-synthase
217 (*CYSTS*) did not show any significance in their effect under flux enforcement. Additional
218 statistical analysis showed that most of the reactions listed in *Supplementary File S4* (27 out
219 of 29) also showed significant differences in the magnitude of their effects among the three
220 different viruses. In other words, whilst the reactions we highlight are not necessarily unique
221 when comparing amongst CHIKV, DENV and ZIKV, their quantitative effects on virus
222 production is significantly different for each individual species. This, combined with the fact
223 that our randomisation process maintained the key features of stoichiometric differences
224 among the host and virus-like biomass functions, highlight that the flux-perturbing effects of

the identified reactions emerge from the core metabolic stoichiometric differences between host and the viruses. In particular, the fact that viruses use much higher levels of nucleic acids per biomass unit (Figure 1).

Many of the predicted additional host reactions effecting virus production can be targeted by existing drugs. Considering the computationally predicted potential of the additional reactions identified as antiviral targets, we have searched for these reactions in a database of known inhibitor-like molecules (31). We found that 15 of these reactions already have known molecules, and in some cases existing drugs, targeting their catalysing enzymes (Figure 3, and full list in *Supplementary File S4*). These findings present experimentally testable predictions on host reactions, the disruption of which could limit virus production. It must be noted, however, that our computational analysis identifies flux enforcement based on differences in host- and virus-optimal states of the model, where 'enforcement' can mean either reduction or increase in a given flux. In contrast, most of the currently known molecules act as enzyme inhibitors (31) and would be expected to reduce metabolic fluxes.

DISCUSSION

We present a computational approach that combines application of FBA and FVA with development of integrated host-virus metabolic models. We show that this novel approach recovers the known metabolic antiviral targets within a human macrophage cell and predicts new potential targets. These predicted reactions fall primarily onto pathways involving nucleotides and amino acids that are differentially used by the host and virus. The results of this study are in line with an integrated perspective that views the virus as an additional metabolic burden on the host cells that could be met or avoided by tinkering of host metabolic fluxes. The observed overlap between predicted reactions and known antiviral

drugs gives confidence to this integrated modelling approach and highlights its potential as a rapid prediction tool to guide experimental design. This can be especially useful in the case of new and emerging viruses for which limited clinical and experimental data may be available to inform drug target identification.

The integrated stoichiometric metabolic modelling approach focuses on metabolic changes as a driver of virus production, and does not consider factors associated with virus-host cell recognition, viral entry and release (32). Furthermore, the application of the linear optimisation on stoichiometric models (i.e. FBA and FVA) strictly assumes that host metabolism is at steady state, and thus prohibits analysis of the dynamics of cellular physiology. Such dynamics could be taken into account to a certain extent by imposing different flux constraints, which could be derived from proximal experimental data (16), through development of simplified metabolic temporal models (10, 11), or by combining dynamics with linear optimisation on stoichiometric models (33, 34). Additionally, the extent of the missing information in genome-scale stoichiometric models creates limitations on how much of the metabolic processes can be covered (35).

The future efforts into model curation and standardisation (36) would open up the possibility of extensive analysis of host-virus pairings from a metabolic stance. The presented findings already suggest that targeting host metabolic processes that are linked to host-virus compositional mismatches can be used to combat virus production without altering host functions. In particular, analysis of extended flux enforcement strategies such as flux limitations on double and triple reaction combinations might identify virus specific drug combinations. Combined with the future development of additional host-virus integrated

274 models covering many cell and virus types can thus allow a fruitful route to computational
275 guiding of experimental antiviral drug discovery.
276
277 **METHODS**
278 **Generation of virus biomass objective functions.** To implement the FBA approach to
279 studying virus infections from a metabolic stance, we define a pseudo reaction accounting for
280 the production of virus particles from its constituents. We call this reaction a virus biomass
281 objective function (VBOF). To account for metabolic fluxes associated with the virus
282 production, the VBOF needs to capture the stoichiometry of nucleotide, amino acid and
283 associated energy metabolites relating to virus production, similar to biomass production
284 function used for microbial metabolic models (37). We derive the metabolic stoichiometry of
285 virus production from the viral genome sequence, the subsequently encoded proteins, the
286 copy number of those proteins, and knowledge of the energetic requirements for peptide
287 bonds and phosphodiester bonds. Details of this derivation is given below, while a schematic
288 of VBOF generation is included as Figure S1.
289 ***Genome and protein information for the viruses.*** The genome sequences used in the
290 present study are obtained from the NCBI genomic database (38) using the following
291 accession numbers and accessed in March 2016; Zika; NC_012532.1, Dengue;
292 NC_001474.2, and CHIKV; NC_004162.2 (original files are provided as *Supplementary File*
293 *S7*). Viruses can be classified by their replication methods, known as the Baltimore
294 Classification System (39), and depending on this classification, a viral particle may contain
295 more than a single copy of the genome. This is factored into the calculation of the nucleotide
296 counts. In the presented study, all studied viruses fall into Group IV classification: they
297 replicate their positive single-stranded RNA (+ssRNA) genome via a negative ssRNA (-
298 ssRNA) intermediate. Therefore, the counts of the nucleotides in the negative strand is equal

to the counts of the complementary nucleotide in the positive strand, i.e. count of A on (+/-) strand = count of U on (-/+) strand, and similarly for G and C counts. The count for each RNA nucleotide (Adenosine (A), Cytidine (C), Guanine (G) and Uracil (U)) can be taken directly from the virus genome sequence: RNA utilises Uracil (U) in place of Thymine (T), therefore T must be replaced with U from the genome sequence readout. In this study, all the viruses have two categories of polyproteins that compose the proteome: structural and non-structural. The amino acid sequence of these two polyproteins, and indeed any genome derived protein sequences, are obtained from gene annotations of the viral genomes as provided in the NCBI genome entries (see above for NCBI entries used). The different sub-categories of the viral proteome may be differentially incorporated into a single virus particle. For the viruses studied here, the structural and non-structural polyproteins are expressed in a ratio that is derived from the overall virus structure (i.e. proteins in the capsid, nucleocapsid, etc.)(18). The ratio is 1:240 for CHIKV(18), and 1:180 for DENV/ZIKV (17). More broadly, the ratio of different protein classes in a single virus particle can be derived from the overall virus structure or directly from literature / experimental evidence.

Calculating nucleotide investment per virus. The total moles of each nucleotide in a mole of virus particle (N_i^{TOT}) are obtained from their count in the virus genome (N_i^G) and replication intermediates (N_i^R), and multiplied by the genome copy number (C_g):

$$N_i^{TOT} = C_g\left(N_i^G + N_i^R\right) \quad (1)$$

where the indexation is over nucleotides. The moles of nucleotides are then converted into grams of nucleotide per mole of virus ($g_{NTPS}\, mol^{-1}{}_{virus}$; G_i^N), by multiplying N_i^{TOT} with the respective molar mass (g mol^{-1}) of the nucleotides (M_i^N):

$$G_i^N = N_i^{TOT} M_i^N \quad (2)$$

where the indexation is over nucleotides. Summing G_i^N over all nucleotides and combining this with the similar calculation for amino acids allows us to get the total molar weight of the virus in terms of nucleotides and amino acids (M_v , see Equation 15 below). Finally, the stoichiometric coefficients of each nucleotide in the VBOF are expressed as millimoles per gram of virus ($mmol_{NTPS}\ g^{-1}{}_{virus}$; S_i^N):

$$S_i^N = 1000\left(\frac{N_i^{TOT}}{M_v}\right) \tag{3}$$

where the indexation is over nucleotides.

Calculating amino acid investment per virus. The total moles of each amino acid per mole of virus particle (X_j^{TOT}) is obtained similarly using the sequence information of structural (X_j^{SP}) and non-structural (X_j^{NP}) proteins. Counts of each amino acid in these proteins is multiplied by the respective copy numbers of these proteins (C_{sp} and C_{np}):

$$X_j^{TOT} = C_{sp}\left(X_j^{SP}\right) + C_{np}\left(X_j^{NP}\right) \tag{4}$$

where the indexation is over amino acids. C_{np} is 1 for all viruses studied here, while C_{sp} is 240 for CHIKV (18), and 180 for DENV/ZIKV (17). The moles of amino acids per mole of virus is then converted into grams of amino acid per mole of virus ($g_{AA}\ mol^{-1}{}_{virus}$; G_j^X), by multiplying X_j^{TOT} with the respective molar mass (g mol^{-1}) of each amino acid (M^X):

$$G_j^X = X_j^{TOT} M_j^X \tag{5}$$

where the indexation is over amino acids. Finally, the stoichiometries of each amino acid in the VBOF is expressed as millimoles per gram of virus ($mmol_{AA}\ g^{-1}{}_{virus}$; S_j^X):

$$S_j^X = 1000\left(\frac{X_j^{TOT}}{M_v}\right) \tag{6}$$

where the indexation is over amino acids.

Calculating ATP requirement for amino acid polymerisation (mmol $g^{-1}{}_{virus}$). The polymerisation of amino acid monomers requires approximately 4 ATP molecules per

peptide bond (40), defined here as the constant k_{ATP} (= 4) The overall moles of ATP (A^{TOT}) required to form the structural (A^{SP}) and non-structural (A^{NP}) polyproteins are calculated from the respective amino acid counts:

$$A^{SP} = \left(\sum_j X_j^{SP} \cdot k_{ATP}\right) - k_{ATP} \tag{7}$$

$$A^{NP} = \left(\sum_j X_j^{NP} \cdot k_{ATP}\right) - k_{ATP} \tag{8}$$

$$A^{TOT} = C_{sp}(A^{SP}) + C_{np}(A^{NP}) \tag{9}$$

where the indexation is over amino acids. From A^{TOT}, we calculate the stoichiometry of ATP in the VBOF as millimoles per gram of virus (S^{ATP}):

$$S^{ATP} = 1000\left(\frac{A^{TOT}}{M_v}\right) \tag{10}$$

As ATP is hydrolysed in this process, the water requirement for polymerisation (S^{H_2O}) is equal to that of ATP. The products from the hydrolysis of ATP (ADP, P_i and H^+) are also accounted for in the VBOF (see Equation 16).

Calculating pyrophosphate (PP_i) liberation from nucleotide polymerisation (mmol g^{-1}_{virus}). The polymerisation of nucleotide monomers to form the RNA viral genome liberates a PP_i molecule (40), defined here as the constant k_{PPi} (= 1).The overall moles of PP_i (P^{TOT}) required to form the viral genome (P^G) and replication intermediates (P^R) are calculated from the respective nucleotide counts:

$$P^G = \left(\sum_i N_i^G \cdot k_{PPi}\right) - k_{PPi} \tag{11}$$

$$P^R = \left(\sum_i N_i^R \cdot k_{PPi}\right) - k_{PPi} \tag{12}$$

$$P^{TOT} = C_g(P^G + P^R) \tag{13}$$

353 To convert this into the PP_i stoichiometry in the VBOF as millimoles per gram of virus (S^{PPi}),
354 we again use the overall molar mass (g mol^{-1}) of one mole of virus:

$$S^{PPi} = 1000\left(\frac{P^{TOT}}{M_v}\right) \tag{14}$$

355 ***Calculating total Viral Molar Mass.*** The total molar mass of the virus M_v is
356 calculated from the total mass of the genome and proteome components as:

$$M_v = \left(\sum_i G_i^N\right) + \left(\sum_j G_j^X\right) \tag{15}$$

357

358 ***Final Construction of the VBOF.*** The left- and right-hand terms of VBOF are based
359 on the above calculations of stoichiometric coefficients. The final stoichiometry for the
360 VBOF (pseudo-reaction) is:

$$S_i^N + \cdots + S_j^X + \cdots + S^{ATP} + S^{H_2O} \rightarrow S^{ADP} + S^{P_i} + S^{H^+} + S^{PPi} \tag{16}$$

361 This pseudo-reaction accounts for the virus' biomass, and the energy requirements associated
362 with its production, and can be incorporated into stoichiometric metabolic models of the host
363 to represent the presence of a virus in that system.

364

365 **Integration of iAB-AMØ-1410 and Chikungunya, Dengue and Zika Viruses.** The VBOFs
366 for the three viruses (CHIKV, DENV, and ZIKV) were integrated into three-separate
367 instances of the 'host' macrophage model (iAB-AMØ-1410) (original files are provided as
368 *Supplementary File S7*). In each individual case, the respective VBOF was appended into the
369 existing macrophage model, with a lower flux bound of zero and an upper bound of infinity,
370 reflecting no upper constraints on this flux (41). No other metabolites or reactions were added
371 to any of the models. All of the individual flux bounds of the model reactions were used as

372 previously set (24), but any bounds set to -1000 or 1000 are replaced with infinity, since the
373 use of infinity, rather than arbitrarily large values, is shown to be a more robust approach to
374 represent unbounded reactions in a linear programming model (41). We also confirmed that
375 the use of arbitrary large bounds (such as -1000/1000) instead of infinity does not change the
376 presented results qualitatively. A set of subprocesses, derived from known aggregate-
377 subsystems (42), were appended as metadata to each individual host-virus model and linked
378 with the pre-existing defined subsystems. A full description of the subsystems and mapping
379 of reactions into these are supplied in *Supplementary File S3*. The used integrated model is
380 provided in a computer readable (SBML) format with the publication.
381
382 **Characterising the stoichiometric differences between host and virus**. For both the host
383 (iAB-AMØ-1410) and viruses (CHIKV, DENV and ZIKV) we have pseudo-reactions that
384 capture the metabolic requirements for the maintenance/production of their respective
385 biomass. By comparing these pseudo-reaction stoichiometries, we can quantify the
386 differences in amino acid and nucleotide requirements to fulfil the host or virus objectives.
387 To do so, we calculate the fold change in nucleotide and amino acid usage by normalising
388 their individual stoichiometric coefficients against the sum of stoichiometries of all
389 metabolites present in the objective function (other than ATP):

$$\log_2\left(\frac{\left(\frac{\sum_i S_i^V}{\sum_k S_k^V}\right)}{\left(\frac{\sum_i S_i^H}{\sum_k S_k^H}\right)}\right) \quad (17)$$

390 where indexation i is over nucleotides (or amino acids) and k is over all biomass precursors,
391 and the subscript H and V indicate the use of the host and virus biomass functions
392 respectively. A positive value indicates a higher usage for nucleotide (or amino acid) i by the
393 virus than the host, whilst a negative value indicates a lower usage.

Comparison of host- and virus-optimised states. For all analyses, the generated host-virus integrated models were optimised and reaction fluxes predicted using the linear optimisation approach known as flux balance analysis (FBA) (43). Linear optimisation is a mathematical technique that optimises a given function under a set of constraints defined by mathematical inequalities. In the context of metabolic models, the constraints correspond to limitations on reaction fluxes, while the function to be optimised can be defined as the flux in a specific reaction. While several biologically plausible objective functions can be defined (44), a common approach is to define a pseudo reaction that describes biomass production from its constituent parts, and then optimise the flux to this reaction, as we have done here. Since the set of constraints includes constraints on uptake reactions, this application of FBA results in prediction of optimal biomass production flux with respect to a specific uptake flux. In other words, FBA optimises for biomass yield from given substrates assumed to be present in the media. In this work, we apply FBA to optimise a combined host-virus metabolic system satisfy either the host or virus objective function (as described above) and study the resulting flux predictions.

To simulate a virus-optimal state, the models are optimised using the respective VBOFs of CHIKV, DENV and ZIKV viruses as the objective function, while to simulate a host-optimal state the models are optimised using the existing biomass maintenance reaction for the human macrophage as presented in (24). Besides running linear optimisation to find the optimal flux sets under each scenario, we have also performed a flux variability analysis (FVA) (45), which provides flux ranges for each reaction that still would allow attainment of a given host/virus optima. The FVA approach is shown to be more robust to instabilities associated with prediction and comparison of a single optimal flux sets (41). For each reaction in the model we compared the resulting flux ranges from FVA under host and virus

419 optimisation, by evaluating the mean value of the allowed flux range for each individual
420 reaction (A_i) and then collating the mean flux values for reactions associated with given
421 subprocesses (aggregated subsystems) as a percentage of total flux through that process.
422 More formally, we define the differential distribution of reaction flux for each subprocess (i)
423 between the host and virus optimised models in terms of a fold-change:

$$\log_2\left(\frac{\left(\frac{\sum_m A_i^V}{\sum_k A_k^V}\right)}{\left(\frac{\sum_m A_i^H}{\sum_k A_k^H}\right)}\right) \quad (18)$$

424 where the indexation k is over all reactions of the model, while the indexation m is over
425 reactions that belong to subprocess i. The superscript indicates the use of flux values from
426 host (H) and virus (V) optimised models respectively. A positive value indicates a higher
427 mean flux in subprocess i in the virus- vs. host-optimised model, whilst a negative value
428 indicates a lower mean flux.
429
430 **Reaction knockout and host-derived flux analyses.** To find reactions which can
431 preferentially alter virus optimised state of the model, we considered the effect of
432 systematically constraining individual reactions. ***Knockout analysis.*** Knockout analysis
433 considers the effect of systematically setting individual reaction fluxes to zero, and then
434 attempting to maximise for VBOF. The knockout optima for the virus production reaction
435 flux Z_{ko} is then compared to the original flux over this reaction; Z_{wt}. ***Host-Derived***
436 ***Enforcement.*** Host-derived enforcement considers the effect of maintaining a metabolic
437 system in a host-optimised state, whilst attempting to optimise the model for VBOF. For this
438 approach, we systematically set individual lower and upper flux bounds of individual
439 reactions to a specific flux range. For each reaction, this range (ε^r) is derived from the
440 corresponding minimum (F^-) and maximum (F^+) flux values for that reaction obtained from

441 the FVA using the host (H) and virus (V) optimisation (as described above). The range (ε^r) is
442 bounded by minimum (ε^-) and maximum (ε^+) flux values, which are given by the following
443 conditional arguments:

$$\begin{aligned} &if \quad F_H^+ > F_V^+, F_H^- \geq F_V^- \\ &then \quad \varepsilon^+ = F_H^+ \\ &\varepsilon^- = F_H^+ - \left(\frac{F_H^+ - F_V^+}{2}\right) \end{aligned} \tag{19}$$

444

$$\begin{aligned} &if \quad F_H^- < F_V^-, F_H^+ \leq F_V^+ \\ &then \quad \varepsilon^- = F_H^- \\ &\varepsilon^+ = F_H^- - \left(\frac{F_H^- - F_V^-}{2}\right) \end{aligned} \tag{20}$$

445

$$\begin{aligned} &if \quad F_H^- > F_V^-, F_H^+ < F_V^+ \\ &then \quad \varepsilon^- = F_H^- \\ &\varepsilon^+ = F_H^+ \end{aligned} \tag{21}$$

446 These calculated flux ranges for each individual reaction are then used to constrain the model
447 and the model is optimised for the VBOF. The resulting optima for the virus production
448 reaction flux; Z_e is recorded and compared to the original optimal value; Z_{wt}.
449
450 **Generation of alternative virus VBOFs and statistical analyses.** The presented approach
451 evaluates the optimisation of host metabolic fluxes for virus production and how such an
452 optimal state can be altered by specific constraints in the host model. To evaluate the impact
453 of having different VBOFs on the outcome of such an analysis, we have generated a range of

VBOFs that were either derived from the original VBOFs or were completely randomly generated. To evaluate impact of small deviations from the original VBOFs, we generated variants of the original virus genomes through nucleotide substitution; for each virus we generated 1000 genome variants, where each variant contained 1, 2, 3, 4, 5 or 10 nucleotide substitutions. For the subsequent VBOF generation from these variant genomes, the genome and protein copy numbers were kept as in the original. To evaluate more variant VBOFs, we generated another 1000 genomes for each virus that were created from the original genome with a random number (between 0 and the total length of the genome) of nucleotide substitutions, and using randomly drawn structural and non-structural polyprotein copy numbers per virus particle. Finally, and in an attempt to generate a set of VBOFs that are far removed from the original ones, both in terms of genome sequence and the structural and non-structural protein numbers, we directly generated random VBOFs. We have implemented this by drawing 1000 sets of individual stoichiometries of biomass components from a uniform distribution on [a, b], where a and b are **1)** ±99% of the original stoichiometric coefficients of a given virus, or **2)** are ±99% of the average of all original stoichiometric coefficients of a given virus. These approaches to generating variant virus genomes give us set of sequences (and associated VBOFs) that are increasingly removed from the original virus VBOFs. For each randomised VBOF created, the host-derived flux enforcement analysis was repeated (with a recalculation of the bounds used for the individual enforcements) and the reactions that perturb virus optima the most when constrained were identified. This whole analysis resulted in 8000 randomised VBOFs and FBA simulations, the results of which are summarised as percentage impact of individual host reactions on virus optima for different sets of VBOFs (see *Supplementary File S5*). To compare results of flux enforcement analysis to that obtained from using randomised biomass functions, we used a one-way ANOVA and Tukey's honest significance tests for each individual virus against

479 the randomised virus group, and between each individual virus species (*Supplementary File*
480 *S6*).

481
482 **Measuring impact of alternative host model assumptions.** As explained above, the
483 presented analysis involves integrating a VBOF into a host model. While we used here a
484 validated, published human macrophage metabolic model as the host model, it is desirable to
485 evaluate the impact of specific assumptions of such a model on the results of this analysis. In
486 particular, the macrophage model uses specific metabolite uptake fluxes, which are mostly
487 based on experimental observations (24), but which can directly influence FBA-based results.
488 To evaluate the potential impact of model uptake bounds, we re-analysed virus optimisation
489 and its constraining by the host model, using alternative metabolite uptake fluxes in the host
490 model in a systematic fashion. We first identified metabolites that are supplied (via exchange
491 reactions) to the metabolic model with non-arbitrary lower bounds (*lb*), where $0 > lb > -\infty$.
492 Each of the identified reactions are then systematically constrained, such that the *lb* is
493 reduced from the original model values (24) (in steps of 10%) until the $lb = 0$, effectively
494 knocking-out the respective exchange reaction. For each altered (additionally constrained)
495 model, the host-derived enforcement analysis is repeated, with re-calculation of the viable
496 host reaction bounds and optimisation of VBOF. This is done for each of the three viruses
497 (CHIKV, DENV, ZIKV) and the results are summarised in *Supplementary File S5*.

498
499 **Supplementary Information** is linked to the online version of the paper.

500 **Acknowledgements** This work was funded by the Defence Science and Technology
501 Laboratory (DSTL). The funders did not have any influence in the design of experiments and
502 analysis of the data. We acknowledge insightful discussions with Lyn O'Brien, James
503 Findley from the DSTL and with Kalesh Shasidharan and other members of the OSS group.

Author Contributions OSS and SA designed and performed the research. MST involved in the original research ideas leading to this study, and both MST and AS have contributed to the interpretation of the results. All authors contributed to the writing of the manuscript.

Author Information The authors declare no competing financial interests. All analyses are performed using an author-developed package written in Python; the ViraNet. This analysis tool is available under an academic, non-commercial use licence on author webpages at http://osslab.lifesci.warwick.ac.uk/?pid=resources. Correspondence and requests for materials should be addressed to OSS (O.Soyer@warwick.ac.uk).

Figures and Figure Legends

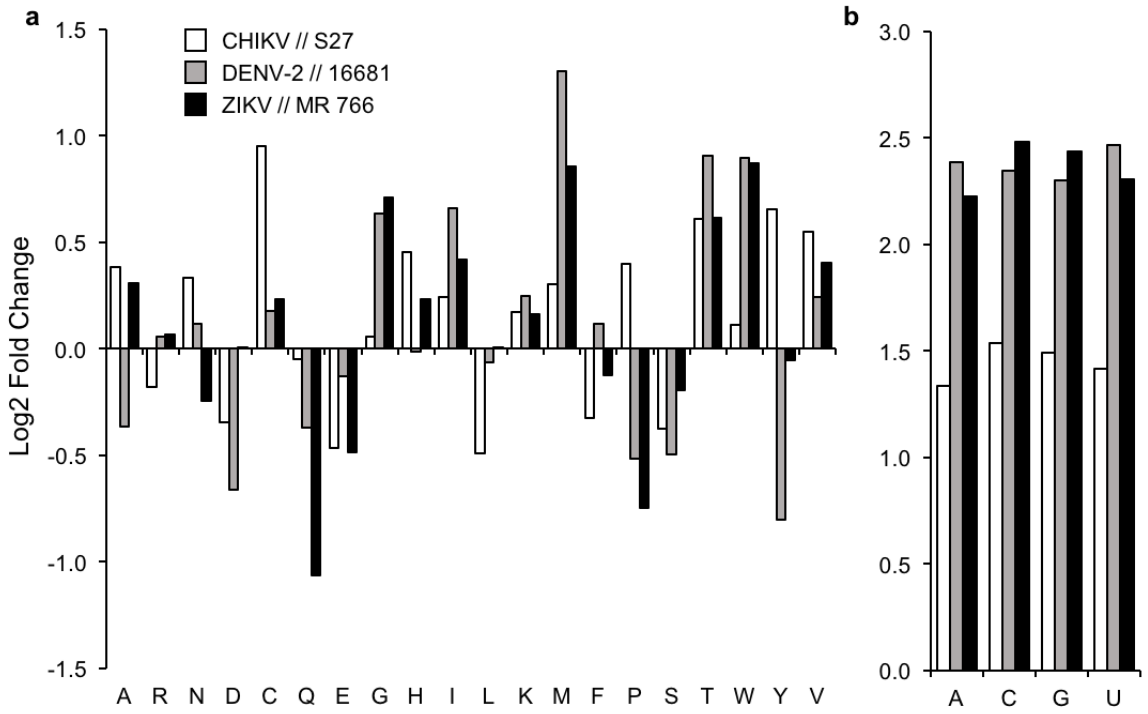

Figure 1 | Fold change difference in usage of amino acids and nucleotides between host and CHIKV, DENV, and ZIKV. a, b, The usage of amino acids (**a**) and nucleotides (**b**) between the host and virus biomass objective functions. The differential usage was calculated against all biomass precursors. Comparison was conducted for all 20 amino acids, and 4 RNA nucleotides (the x-axes are labelled with the common short notations for these). All calculations and biomass formulations are as described in the *Methods*, and all biomass stoichiometric values are provided as *Supplementary File S1*.

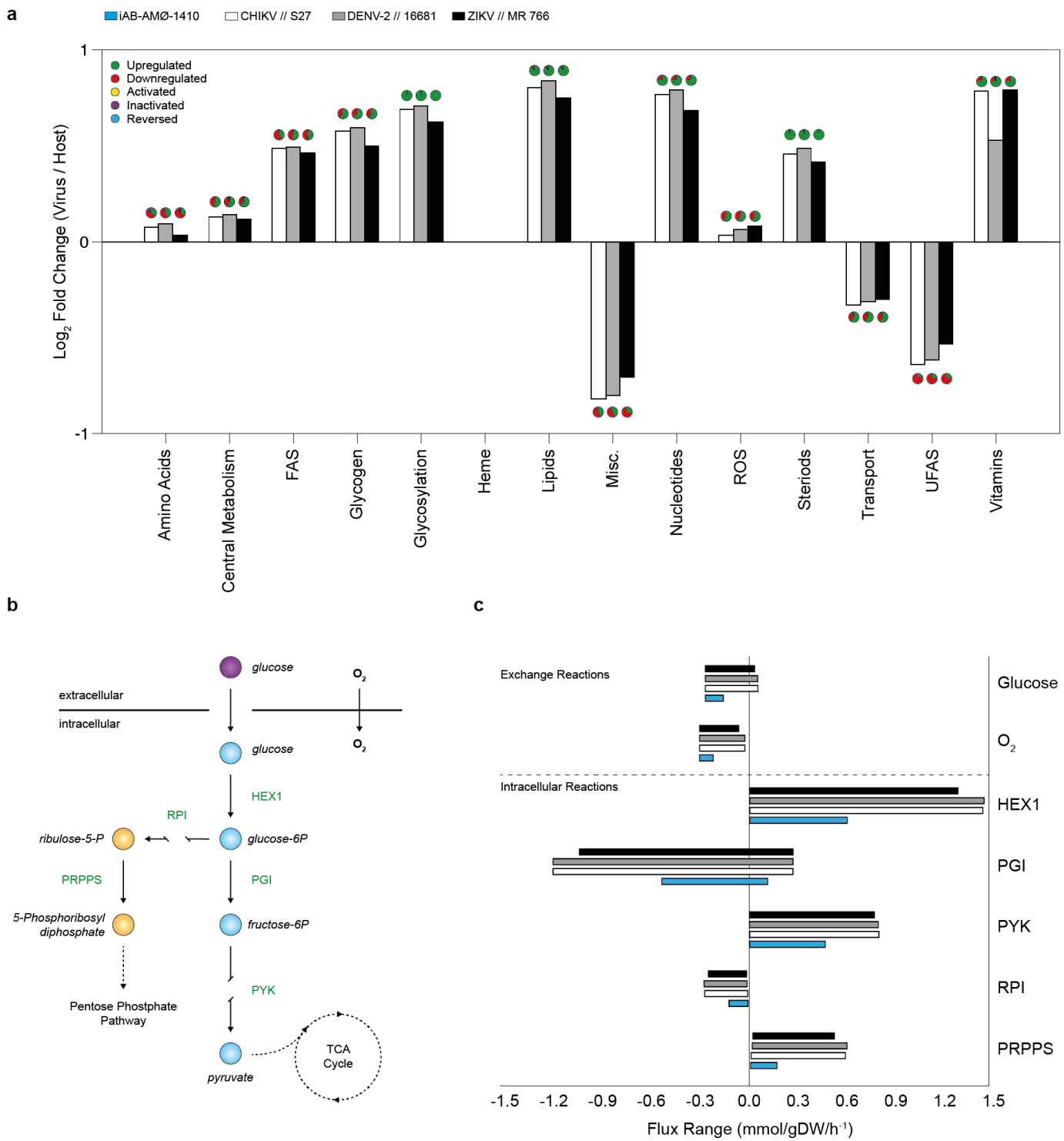

Figure 2 | Comparison of model fluxes between host optima and CHIKV, DENV and ZIKV optima. a, Comparisons are visualised as the sum of fluxes over aggregated subsystems using values from host- and virus-optimal states. Abbreviations used in the subsystem classification are: FAS, Fatty Acid Synthesis; ROS, Reactive Oxygen Species; UFAS, Unsaturated Fatty Acid Synthesis; Misc., Miscellaneous. The *y*-axis represents

526 differential usage of aggregate subsystems, while the colours of the bars indicate different
527 viruses and host (see colour coding on the panel). Positive and negative values reflect a
528 higher or lower total flux for that subsystem in the virus- compared to host-optimal state. Pie-
529 charts over each bar provide a summary of changes on individual reactions within a
530 subsystem. The complete set of flux values for all reactions in the model and for all optimal
531 states are provided as *Supplementary File S1*. **b,** Simplified schematic showing reactions
532 involved in the glycolysis pathway. **c,** Corresponding flux ranges of individual reactions, in
533 the glycolysis pathway, that allow attainment of host- and virus-optima. The flux ranges
534 allowing optima for individual viruses, as well as the host are shown in differentially
535 coloured bars with the *x*-axis showing flux values. The colour coding is as shown in panel **a**.
536

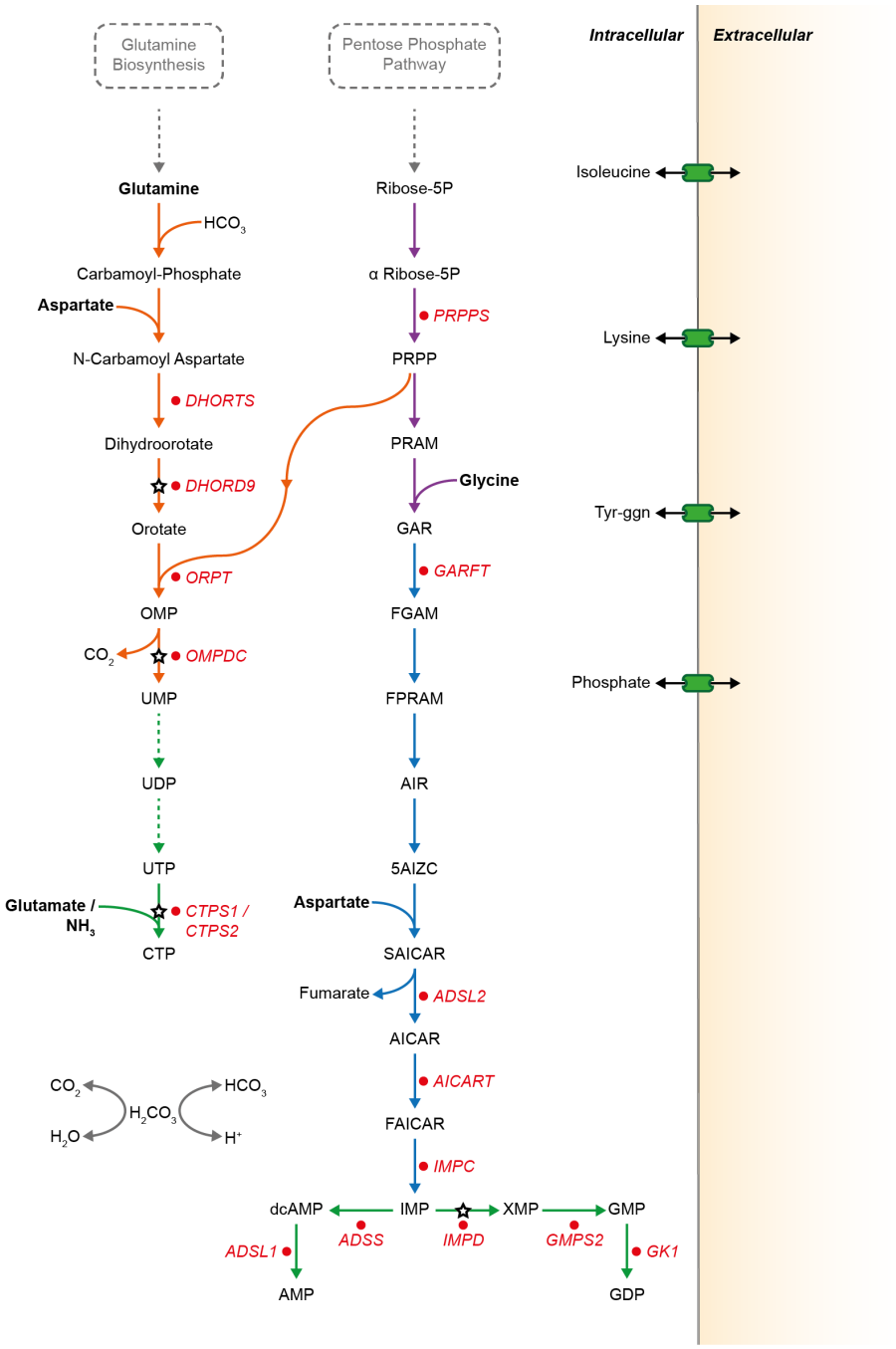

Figure 3 | Reaction pathway schematic showing the top 29 reactions from host-derived flux enforcement analysis and their associated antiviral drugs and inhibitors. Key reactions inhibiting virus-optima when flux ranges derived from host and virus flux variability analysis are enforced (the same reactions listed in *Supplementary File S4*). Abbreviations used for the compounds and reactions are as in *Supplementary Table S2* and *S3* respectively. Some of the identified reactions are interconnected, forming pathways. Pathways associated with subsystems are indicated by coloured reaction arrows: Orange,

545 pyrimidine synthesis; Purple, pentose phosphate pathway; Blue, purine synthesis; Green,
546 nucleotide biosynthesis. The starting metabolites into these pathways, Glutamine and D-
547 Ribose 5-phosphate, are derived from glutamine biosynthesis and pentose phosphate
548 pathways. Reactions targeted by a known antiviral or inhibitor are marked by white and red
549 filled stars and circles, respectively. Complete list of antiviral compounds from which the
550 matches were obtained are provided as *Supplementary Table S1*. Complete list of inhibitors
551 and the associated reactions are provided as *Supplementary File S4*. A complete list of
552 enforcement results for all reactions are provided as *Supplementary Files S2* and *S5*.
553 .
554
555

556 **Supplementary Files**

557 **Supplementary File S1.** Metabolites and their associated stoichiometric coefficients for the
558 [host] macrophage (iAB-AMØ-1410) biomass maintenance objective function and the
559 Chikungunya (CHIKV), Dengue (DENV) and Zika (ZIKV) virus biomass objective
560 functions.

561

562 **Supplementary File S2.** FVA results for the host-virus integrated models for CHIKV,
563 DENV and ZIKV. Results obtained from either using the host- or virus-optimization are
564 shown. Model reactions, model subsystems and the associated aggregated subsystems are
565 also detailed.

566

567 **Supplementary File S3.** Results for the reaction knockout and host-derived enforcement
568 analyses. For each reaction alteration (knockout or flux enforcement), the resulting virus
569 optima, for CHIKV, DENV and ZIKV, are shown as a percentage of the original model
570 (without the additional constraints imposed by the analyses). The lower and upper flux
571 bounds used for the host-derived enforcement analysis are listed for the relevant reaction and
572 associated virus optimisation result. Model reactions and model subsystems are also listed

573

574 **Supplementary File S4.** A list of model reactions identified from the host-enforcement
575 analysis that are able to reduce the optimal flux for one of the three viruses, CHIKV, DENV
576 and ZIKV, to below 80% of the original (obtained from the original model). Inhibitors are
577 listed for the respective reactions, and were identified through the Brenda Enzymatic
578 Database via the Enzyme Commission Number associated with the reaction.

579

580 **Supplementary File S5.** Results of model sensitivity analysis, involving both alterations in
581 media uptake fluxes and virus biomass functions.
582
583 **Supplementary File S6.** Results of statistical analyses on the effect of host-derived
584 enforcements across original, point-mutated, and randomly generated virus biomass
585 functions.
586
587 **Supplementary File S7.** An archived (i.e. zipped) containing: (*i*) the [host] macrophage iAB-
588 AMØ-1410 metabolic model ('macModel.mat'), and the (*ii*) full genbank files, obtained from
589 NCBI, for Chikungunya ('CHIKV.txt'), Dengue ('DENV.txt'), and Zika ('ZIKV.txt')
590 viruses. These files are used to create the virus biomass objective functions and the
591 corresponding integrated host-virus models.
592
593

Supplementary Figures

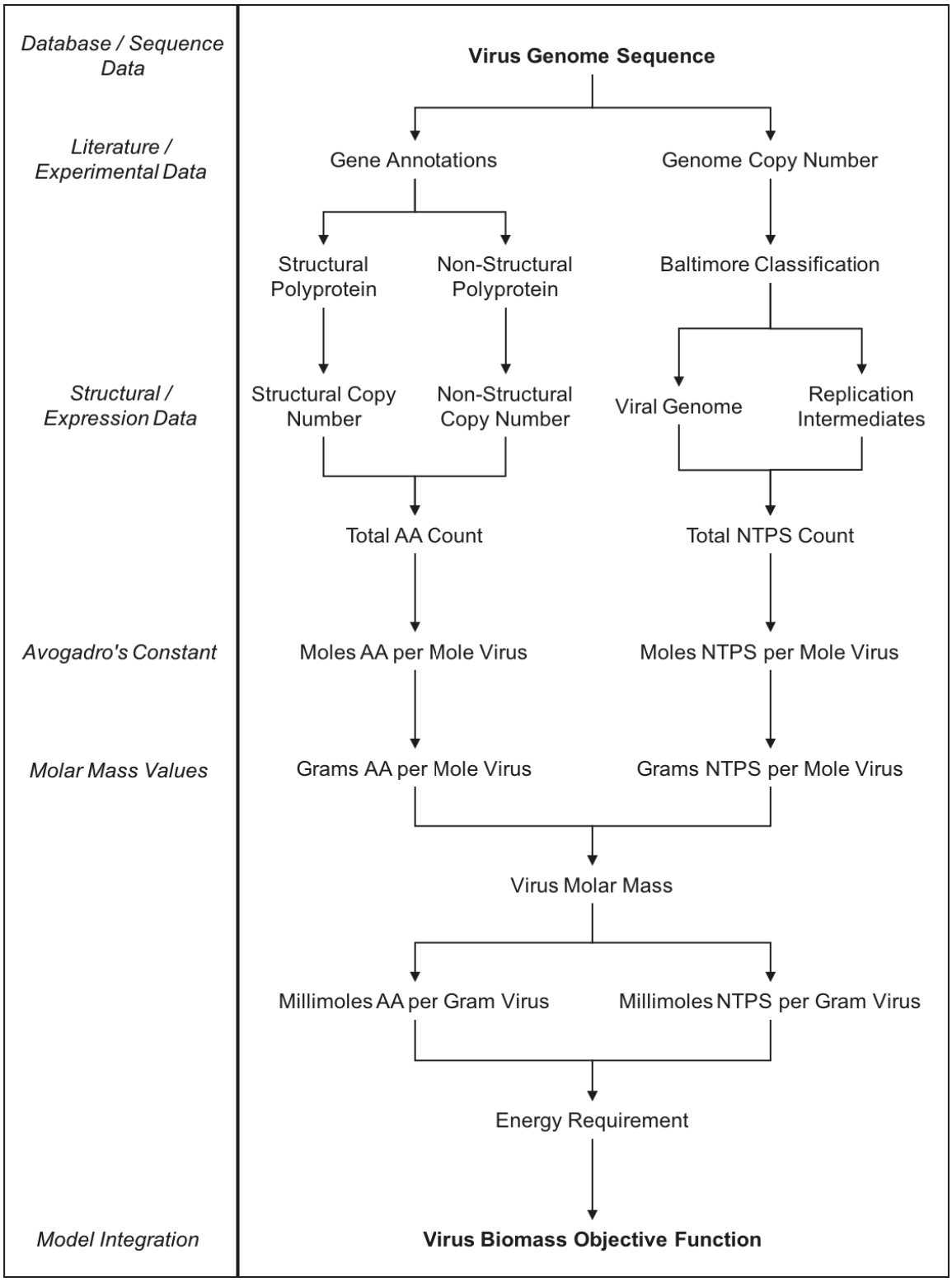

Figure S1 | Schematic of virus biomass objective function (VBOF) generation. Diagram outlines the process of forming the necessary components for the pseudo-reaction that represents the production of virus particles (biomass).

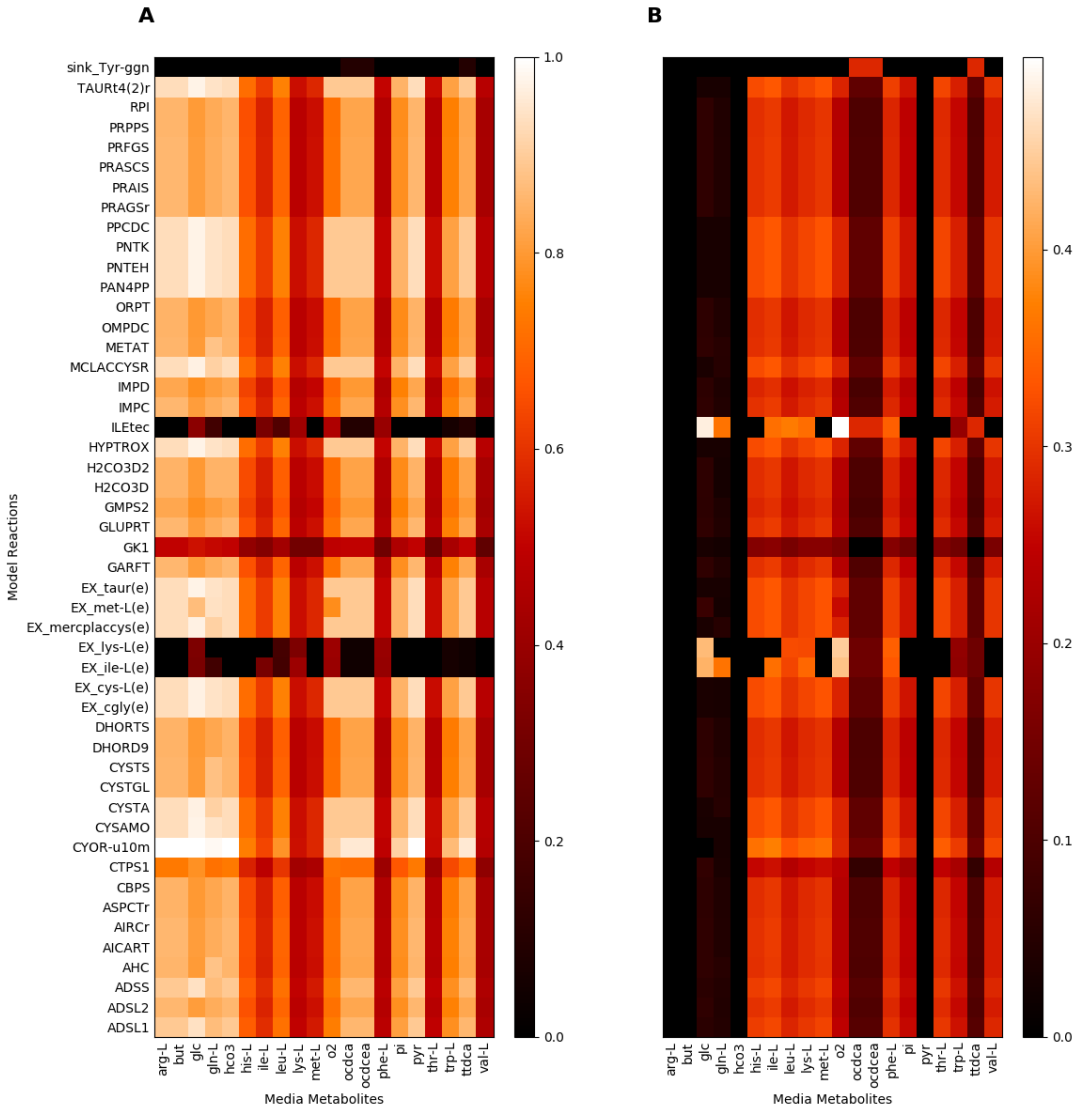

Figure S2 | Host-derived enforcement reactions analysed over varying model media compositions for CHIKV. A) average normalised virus optima for each media alteration condition. B) standard deviation of virus optima for each media alteration condition.

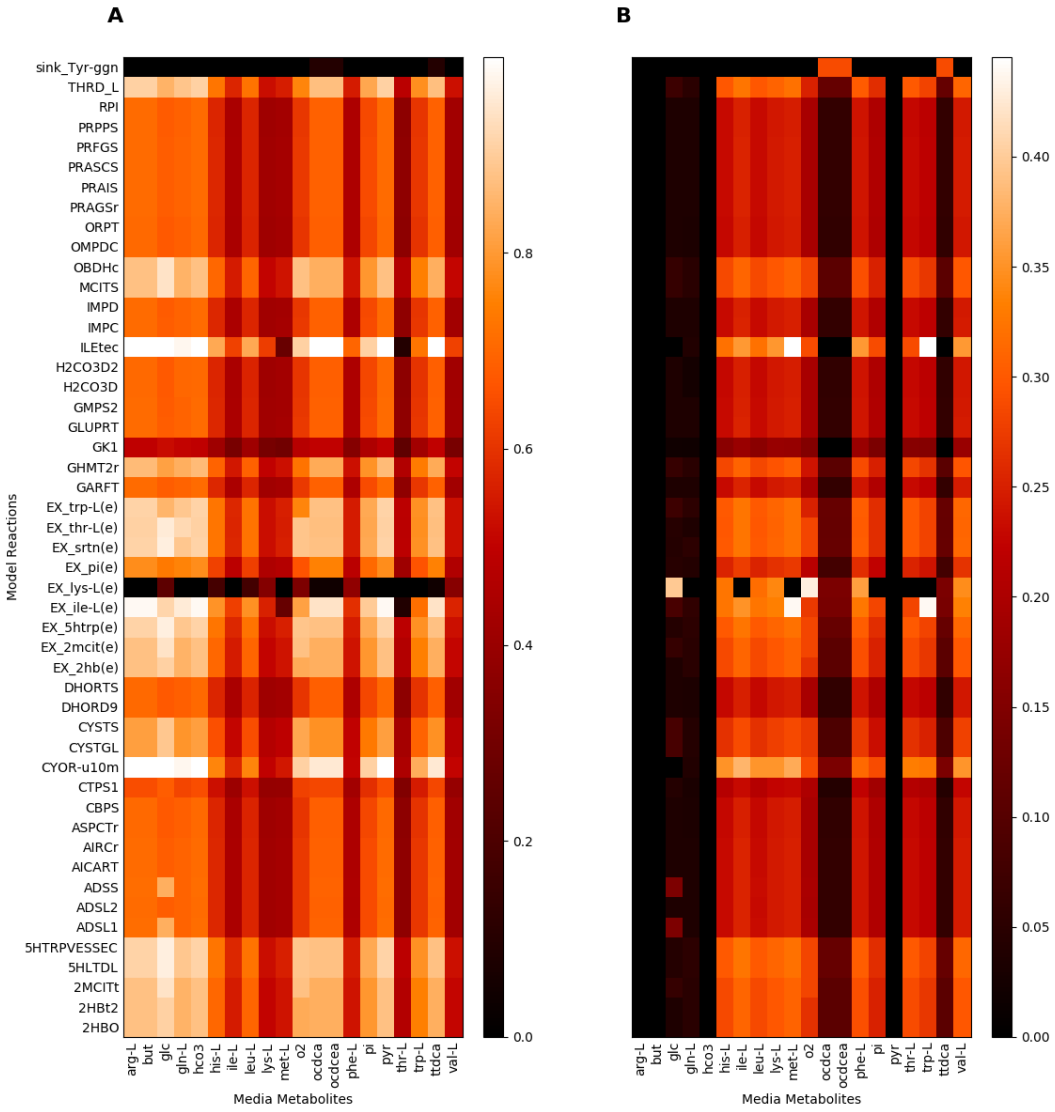

Figure S3 | Host-derived enforcement reactions analysed over varying model media compositions for DENV. A) average normalised virus optima for each media alteration condition. B) standard deviation of virus optima for each media alteration condition.

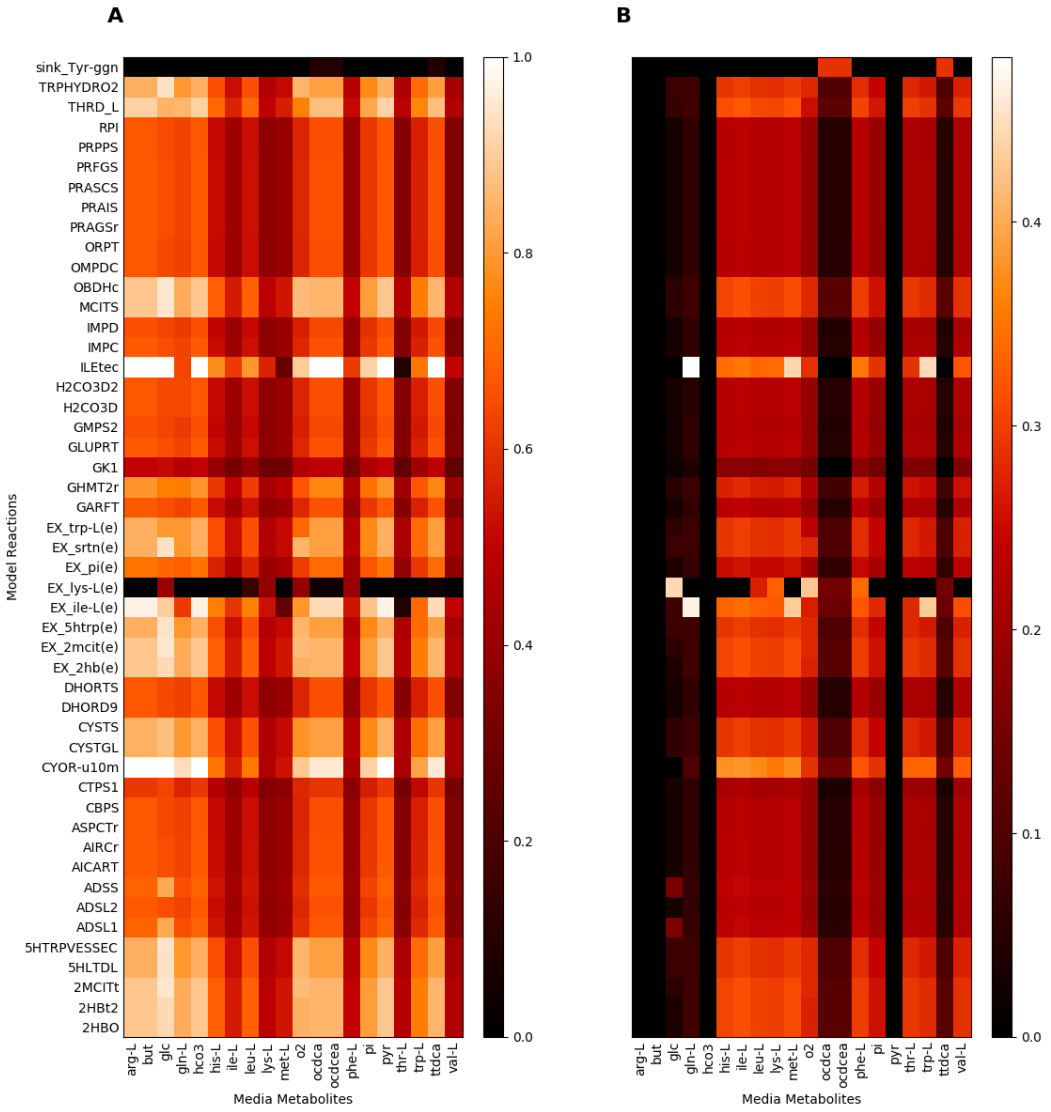

Figure S4 | Host-derived enforcement reactions analysed over varying model media compositions for ZIKV. A) average normalised virus optima for each media alteration condition. B) standard deviation of virus optima for each media alteration condition.

620 **Supplementary Tables**

Compound Identifier	Target Reaction	Model Reaction ID Equivalent	Enzyme Commission Number
Cyclopentylcytosine	Cytidine triphosphate synthetase	CTPS1*	6.3.4.2
Cyclopentenylcytosine	Cytidine triphosphate synthetase	CTPS1*	6.3.4.2
DD264	Dihydroorotate dehydrogenase	DHORD9	1.3.5.2
NITD-982	Dihydroorotate dehydrogenase	DHORD9	1.3.5.2
A3	Dihydroorotate dehydrogenase	DHORD9	1.3.5.2
Ribavirin	Inosine 5'-monophosphate dehydrogenase	IMPD	1.1.1.205
VX-497	Inosine 5'-monophosphate dehydrogenase	IMPD	1.1.1.205
Pyrazofurin	Orotidine 5'-phosphate decarboxylase	OMPDC	4.1.1.23
6-azauridine	Orotidine 5'-phosphate decarboxylase	OMPDC	4.1.1.23
C-c3Ado	S-adenosylhomocysteine hydrolase	AHC	3.3.1.1
neplanocin A	S-adenosylhomocysteine hydrolase	AHC	3.3.1.1
3-deazaneplanocin A	S-adenosylhomocysteine hydrolase	AHC	3.3.1.1
aristeromycin	S-adenosylhomocysteine hydrolase	AHC	3.3.1.1

621

622 **Supplementary Table S1 | List of antiviral compounds identified, which interact with**
623 **host metabolic reactions that affect RNA virus production** (29)

624 * CTP Synthase is encoded for by two genes, CTPS1 and CTPS2, and both are affected by
625 the associated antiviral compounds. Only one gene is shown. All antiviral compounds, and
626 their associated target reactions, were identified from literature search (see Citations).

Metabolite Name	Associated Abbreviation	KEGG Compound Identifier
Orotidine 5-phosphate	OMP	C01103
Uridine monophosphate	UMP	C00105
Uridine diphosphate	UDP	C00015
Uridine triphosphate	UTP	C00075
Cytidine triphosphate	CTP	C00063
5-Phospho-alpha-D-ribose 1-diphosphate	PRPP	C00119
5-Phospho-beta-D-ribosylamine	PRAM	C03090
N1-(5-Phospho-D-ribosyl)glycinamide	GAR	C03838
N2-Formyl-N1-(5-phospho-D-ribosyl)glycinamide	FGAM	C04376
2-(Formamido)-N1-(5-phospho-D-ribosyl)acetamidine	FPRAM	C04640
5-amino-1-(5-phospho-D-ribosyl)imidazole	AIR	C03373
5-amino-1-(5-phospho-D-ribosyl)imidazole-4-carboxylate	5AIZC	C04751
(S)-2-[5-Amino-1-(5-phospho-D-ribosyl)imidazole-4-carboxamido]succinate	SAICAR	C04823
5-Amino-1-(5-Phospho-D-ribosyl)imidazole-4-carboxamide	AICAR	C04677
5-Formamido-1-(5-phospho-D-ribosyl)imidazole-4-carboxamide	FAICAR	C04734
Inosine monophosphate	IMP	C00130
Xanthosine monophosphate	XMP	C00655
Guanosine monophosphate	GMP	C00144
Guanosine diphosphate	GDP	C00035
N6-(1,2-Dicarboxyethyl)-AMP	dcAMP	C03794
Adenosine monophosphate	AMP	C00020
Tyr-194 of apo-glycogenin protein (primer for glycogen synthesis)	Tyr-ggn	*N/A*

Supplementary Table S2 | Metabolite abbreviations and full names used in Figure 3, as derived from the iAB-AMØ-1410 Human Alveolar Macrophage metabolic reconstruction (24)**.**

Model Reaction ID	Model Reaction Name	Enzyme Commission Number
ADSL1	adenylosuccinate lyase (I)	4.3.2.2
ADSL2	adenylosuccinate lyase (II)	4.3.2.2
ADSS	adenylosuccinate synthase	6.3.4.4
AICART	phosphoribosylaminoimidazolecarboxamide formyltransferase	2.1.2.3
CTPS1	CTP synthase (NH3)	6.3.4.2
CTPS2	CTP synthase (glutamine)	6.3.4.2
DHORD9	dihydroorotic acid dehydrogenase (quinone10)	-
DHORTS	dihydroorotase	3.5.2.3
GARFT	phosphoribosylglycinamide formyltransferase	2.1.2.2
GK1	guanylate kinase (GMP:ATP)	2.7.4.8
GMPS2	GMP synthase	6.3.5.2
IMPC	IMP cyclohydrolase	3.5.4.10
IMPD	IMP dehydrogenase	1.1.1.205
OMPDC	orotidine-5-phosphate decarboxylase	4.1.1.23
ORPT	orotate phosphoribosyltransferase	2.4.2.10
PRPPS	phosphoribosylpyrophosphate synthetase	2.7.6.1

Supplementary Table S3 | Reaction abbreviations and full names used in Figure 3, as derived from the iAB-AMØ-1410 Human Alveolar Macrophage metabolic reconstruction (24)**.**

637 **References**

638 1. Littler E, Oberg B (2005) Achievements and challenges in antiviral drug discovery.
639 *Antivir Chem Chemother* 16(3):155–168.

640 2. Mlakar J, et al. (2016) Zika Virus Associated with Microcephaly. *N Engl J Med*
641 374(10):951–958.

642 3. Kotzamanis K, Angulo A, Ghazal P (2015) Infection homeostasis: implications for
643 therapeutic and immune programming of metabolism in controlling infection. *Med*
644 *Microbiol Immunol* 204(3):395–407.

645 4. Maynard ND, et al. (2010) A forward-genetic screen and dynamic analysis of lambda
646 phage host-dependencies reveals an extensive interaction network and a new anti-viral
647 strategy. *PLoS Genet* 6(7):e1001017.

648 5. Merino-Ramos T, et al. (2015) Modification of the Host Cell Lipid Metabolism
649 Induced by Hypolipidemic Drugs Targeting the Acetyl Coenzyme A Carboxylase
650 Impairs West Nile Virus Replication. *Antimicrob Agents Chemother* 60(1):307–315.

651 6. Zhu Y, Yongky A, Yin J (2009) Growth of an RNA virus in single cells reveals a
652 broad fitness distribution. *Virology* 385(1):39–46.

653 7. Yu Y, Clippinger AJ, Alwine JC (2011) Viral effects on metabolism: changes in
654 glucose and glutamine utilization during human cytomegalovirus infection. *Trends in*
655 *Microbiology* 19(7):360–367.

656 8. El-Bacha T, Menezes MMT, Azevedo e Silva MC, Sola-Penna M, Da Poian AT
657 (2004) Mayaro virus infection alters glucose metabolism in cultured cells through
658 activation of the enzyme 6-phosphofructo 1-kinase. *Mol Cell Biochem* 266(1-2):191–
659 198.

660 9. Jain R, Srivastava R (2009) Metabolic investigation of host/pathogen interaction using
661 MS2-infected Escherichia coli. *BMC Syst Biol* 3:121.

662 10. Molenaar D, van Berlo R, de Ridder D, Teusink B (2009) Shifts in growth strategies
663 reflect tradeoffs in cellular economics. *Molecular Systems Biology* 5:323.

664 11. Weiße AY, Oyarzún DA, Danos V, Swain PS (2015) Mechanistic links between
665 cellular trade-offs, gene expression, and growth. *Proc Natl Acad Sci USA*
666 112(9):E1038–47.

667 12. Maynard ND, Gutschow MV, Birch EW, Covert MW (2010) The virus as metabolic
668 engineer. *Biotechnol J* 5(7):686–694.

669 13. Ikeda M, Kato N (2007) Modulation of host metabolism as a target of new antivirals.
670 *Adv Drug Deliv Rev* 59(12):1277–1289.

671 14. Price ND, Papin JA, Schilling CH, Palsson BØ (2003) Genome-scale microbial in
672 silico models: the constraints-based approach. *Trends Biotechnol* 21(4):163–169.

673 15. Terzer M, Maynard ND, Covert MW, Stelling J (2009) Genome-scale metabolic

674 networks. *Wiley Interdiscip Rev Syst Biol Med* 1(3):285–297.

675 16. Birch EW, Ruggero NA, Covert MW (2012) Determining host metabolic limitations
676 on viral replication via integrated modeling and experimental perturbation. *PLoS*
677 *Comput Biol* 8(10):e1002746.

678 17. Mukhopadhyay S, Kuhn RJ, Rossmann MG (2005) A structural perspective of the
679 flavivirus life cycle. *Nat Rev Microbiol* 3(1):13–22.

680 18. Strauss JH, Strauss EG (1994) The alphaviruses: gene expression, replication, and
681 evolution. *Microbiol Rev* 58(4):806–562.

682 19. Fox JM, et al. (2015) Broadly Neutralizing Alphavirus Antibodies Bind an Epitope on
683 E2 and Inhibit Entry and Egress. *Cell* 163(5):1095–1107.

684 20. Gollins SW, Porterfield JS (1985) Flavivirus infection enhancement in macrophages:
685 an electron microscopic study of viral cellular entry. *J Gen Virol* 66 (Pt 9)(9):1969–
686 1982.

687 21. Balsitis SJ, et al. (2009) Tropism of dengue virus in mice and humans defined by viral
688 nonstructural protein 3-specific immunostaining. *Am J Trop Med Hyg* 80(3):416–424.

689 22. Garmashova N, et al. (2007) The Old World and New World alphaviruses use different
690 virus-specific proteins for induction of transcriptional shutoff. *Journal of Virology*
691 81(5):2472–2484.

692 23. Lundström JO (1999) Mosquito-borne viruses in western Europe: a review. *J Vector*
693 *Ecol* 24(1):1–39.

694 24. Bordbar A, Lewis NE, Schellenberger J, Palsson BØ, Jamshidi N (2010) Insight into
695 human alveolar macrophage and M. tuberculosis interactions via metabolic
696 reconstructions. *Molecular Systems Biology* 6:422.

697 25. Chindelevitch L, Trigg J, Regev A, Berger B (2014) An exact arithmetic toolbox for a
698 consistent and reproducible structural analysis of metabolic network models. *Nature*
699 *Communications* 5:4893.

700 26. Delgado T, et al. (2010) Induction of the Warburg effect by Kaposi's sarcoma
701 herpesvirus is required for the maintenance of latently infected endothelial cells. *Proc*
702 *Natl Acad Sci USA* 107(23):10696–10701.

703 27. Khan M, Dhanwani R, Patro IK, Rao PVL, Parida MM (2011) Cellular IMPDH
704 enzyme activity is a potential target for the inhibition of Chikungunya virus replication
705 and virus induced apoptosis in cultured mammalian cells. *Antiviral Research* 89(1):1–
706 8.

707 28. Wang Q-Y, et al. (2011) Inhibition of dengue virus through suppression of host
708 pyrimidine biosynthesis. *Journal of Virology* 85(13):6548–6556.

709 29. Leyssen P, De Clercq E, Neyts J (2008) Molecular strategies to inhibit the replication
710 of RNA viruses. *Antiviral Research* 78(1):9–25.

30. UniProt Consortium (2015) UniProt: a hub for protein information. *Nucleic Acids Research* 43(Database issue):D204–12.

31. Schomburg I (2004) BRENDA, the enzyme database: updates and major new developments. *Nucleic Acids Research* 32(90001):431D–433.

32. Timm A, Yin J (2012) Kinetics of virus production from single cells. *Virology* 424(1):11–17.

33. Birch EW, Udell M, Covert MW (2014) Incorporation of flexible objectives and time-linked simulation with flux balance analysis. *J Theor Biol* 345:12–21.

34. Mahadevan R, Edwards JS, Doyle FJ III (2002) Dynamic Flux Balance Analysis of Diauxic Growth in Escherichia coli. *Biophysical Journal* 83(3):1331–1340.

35. Aurich MK, Thiele I (2016) Computational Modeling of Human Metabolism and Its Application to Systems Biomedicine. *Methods Mol Biol* 1386(Chapter 12):253–281.

36. Zomorrodi AR, Segrè D (2016) Synthetic Ecology of Microbes: Mathematical Models and Applications. *Journal of Molecular Biology* 428(5):837–861.

37. Thiele I, Palsson BØ (2010) A protocol for generating a high-quality genome-scale metabolic reconstruction. *Nature Protocols* 5(1):93–121.

38. Geer LY, et al. (2010) The NCBI BioSystems database. *Nucleic Acids Research* 38(Database issue):D492–6.

39. Yu C, et al. (2013) Real time classification of viruses in 12 dimensions. *PLoS ONE* 8(5):e64328.

40. Haynie DT (2009) *Biological Thermodynamics* (Cambridge University Press, Cambridge). 2nd Ed. doi:10.1017/CBO9780511802690.

41. Kelk SM, Olivier BG, Stougie L, Bruggeman FJ (2012) Optimal flux spaces of genome-scale stoichiometric models are determined by a few subnetworks. *Scientific reports*. doi:10.1038/srep00580.

42. Zielinski DC, et al. (2015) Pharmacogenomic and clinical data link non-pharmacokinetic metabolic dysregulation to drug side effect pathogenesis. *Nature Communications* 6:7101.

43. Orth JD, Thiele I, Palsson BØ (2010) What is flux balance analysis? *Nat Biotechnol* 28(3):245–248.

44. Chiu H-C, Segrè D (2008) Comparative determination of biomass composition in differentially active metabolic States. *Genome Inform* 20:171–182.

45. Mahadevan R, Schilling CH (2003) The effects of alternate optimal solutions in constraint-based genome-scale metabolic models. *Metabolic Engineering* 5(4):264–276.